

Spherical integration in acoustical holography

Puhle, Christof¹

Society for the Advancement of Applied Computer Science, GFaI e.V.
Volmerstraße 3, 12489 Berlin, Germany

ABSTRACT

In this paper, we approach the forward exterior problem of spherical acoustical holography, i.e. all sources are contained within a sphere of certain radius, and, using measurements outside this sphere, sound field predictions are obtained from the surface out to the farfield. In this setup, we propose a reconstruction method that makes extensive use of spherical numerical integration together with an efficient iteration strategy. A characteristic feature of this method is the exact reconstruction of emissions (read: solutions to the Helmholtz equation) up to a certain degree. To render real-life applications possible, we discuss alternatives to a full-spherical measurement. Our considerations include simulations/reconstructions for various source setups including (smoothed) circular spherical cap pistons.

Keywords: Signal processing, sound field predictions, acoustical holography

I-INCE Classification of Subject Number: 74–76

(see <http://i-ince.org/files/data/classification.pdf>)

1. RECONSTRUCTION OF SPHERICAL WAVES

Let $p : \mathbb{R}^3 \rightarrow \overline{\mathbb{C}}$ be the complex amplitude of a time-harmonic sound pressure field of angular frequency $\omega > 0$ and speed of propagation $c > 0$. By definition, p satisfies the Helmholtz equation

$$\frac{\partial^2 p}{\partial x^2} + \frac{\partial^2 p}{\partial y^2} + \frac{\partial^2 p}{\partial z^2} + k^2 p = 0, \quad k = \frac{\omega}{c}. \quad (1)$$

Our sign convention for a time-harmonic function is $t \mapsto \exp(i\omega t)$. For example,

$$p(x, y, z) = \frac{\exp\left(-ik \sqrt{x^2 + y^2 + z^2}\right)}{\sqrt{x^2 + y^2 + z^2}} \quad (2)$$

represents an outgoing spherical wave with source in $(0, 0, 0)$.

¹puhle@gfai.de

Let $\hat{p} : [0, \infty] \times [0, \pi] \times [0, 2\pi] \rightarrow \overline{\mathbb{C}}$ be p 's representation in spherical coordinates (r, θ, ϕ) . Consequently, \hat{p} satisfies

$$\frac{1}{r^2} \frac{\partial}{\partial r} \left(r^2 \frac{\partial \hat{p}}{\partial r} \right) + \frac{1}{r^2 \sin \theta} \frac{\partial}{\partial \theta} \left(\sin \theta \frac{\partial \hat{p}}{\partial \theta} \right) + \frac{1}{r^2 \sin^2 \theta} \frac{\partial^2 \hat{p}}{\partial \phi^2} + k^2 \hat{p} = 0. \quad (3)$$

Solutions to this equation can be found analytically by assuming that \hat{p} is separable, i.e. there exist functions $R : [0, \infty] \rightarrow \overline{\mathbb{C}}$, $\Theta : [0, \pi] \rightarrow \overline{\mathbb{C}}$, $\Phi : [0, 2\pi] \rightarrow \overline{\mathbb{C}}$ such that

$$\hat{p}(r, \theta, \phi) = R(r) \cdot \Theta(\theta) \cdot \Phi(\phi). \quad (4)$$

In this case, equation (3) leads to

$$R(r) = A \cdot h_l^{(1)}(kr) + B \cdot h_l^{(2)}(kr) \quad (5)$$

for some constants $A, B \in \mathbb{C}$, $l \in \mathbb{N}_0 = \{0, 1, \dots\}$, and $h_l^{(1)}, h_l^{(2)}$ denote the spherical Hankel functions of the first and second kind of degree l , respectively. Moreover, we have

$$\Theta(\theta) \cdot \Phi(\phi) = Y_l^m(\theta, \phi), \quad (6)$$

where $m \in \{-l, -l+1, \dots, l\}$, and Y_l^m is the spherical harmonic of degree l and order m .

We now suppose p is generated in the compact ball of radius $r_0 > 0$ centered at $(0, 0, 0)$, its complement

$$D = \{(x, y, z) \in \mathbb{R}^3 : r = \sqrt{x^2 + y^2 + z^2} > r_0\} \quad (7)$$

is supposed to be source free. Motivated by Sommerfeld's radiation condition (see [1]), we then assume that (in the area of interest) \hat{p} is (at least in good approximation) a superposition of the first $(L_0 + 1)^2$ outgoing separable solutions of (3),

$$\hat{p}(r, \theta, \phi) = \sum_{l=0}^{L_0} \sum_{m=-l}^l B_{lm} \cdot h_l^{(2)}(kr) \cdot Y_l^m(\theta, \phi), \quad B_{lm} \in \mathbb{C}. \quad (8)$$

Based on a measurement of \hat{p} at the positions

$$(r_i, \theta_i, \phi_i) \in (r_0, \infty] \times [0, \pi] \times [0, 2\pi], \quad i = 1, \dots, N \quad (9)$$

in the source-free region D , we now discuss a few methods on how to determine/reconstruct the $(L_0 + 1)^2$ complex numbers $B_{lm} \in \mathbb{C}$ numerically.

1.1.1. Least-squares methods

A standard approach to solve the system of equations resulting from (8) is the method of least squares. However, if the degree L_0 of p is not known a priori, this method is highly prone to errors. In this case, the HELS method (see [2]) is a more feasible approach, it determines \hat{p} as follows. Initially, it decomposes the set of measurement indices into two disjoint subsets,

$$\{1, \dots, N\} = I_S \dot{\cup} I_R, \quad \#I_S = \begin{cases} \#I_R & N \text{ even} \\ \#I_R + 1 & N \text{ odd} \end{cases}. \quad (10)$$

Then, for each maximal degree

$$J \in \mathcal{J} \subset \mathbb{N}, \quad \#\mathcal{J} < \infty \quad (11)$$

of outgoing separable solutions under consideration, it determines the least squares solution \hat{p}^J of (8) using the so-called solving positions (r_i, θ_i, ϕ_i) , $i \in I_S$ and computes its error Δ_J at the remaining positions:

$$\Delta_J = \sum_{i \in I_R} |\hat{p}(r_i, \theta_i, \phi_i) - \hat{p}^J(r_i, \theta_i, \phi_i)|^2. \quad (12)$$

Finally, \hat{p} is chosen to be the least squares solution with the smallest error,

$$\hat{p} = \hat{p}^{J_{\min}}, \quad J_{\min} = \arg \min_{J \in \mathcal{J}} \Delta_J. \quad (13)$$

A more elaborate variant of the HELS method utilizing the modified Tikhonov regularization (see [3]) together with the generalized cross-validation (see [4]) is discussed in Wu's book [2].

All these methods share the same drawbacks of the underlying least-squares method when it comes to the estimation of errors in the reconstructed coefficients B_{lm} , especially if L_0 is known only approximately. Moreover – in many real world applications – the number of measurement positions is small compared to the number of parameters to reconstruct,

$$N < (L_0 + 1)^2, \quad (14)$$

leaving the system of equations resulting from (8) underdetermined. We therefore follow a different approach in this article.

1.1.2. Integration on the sphere

In theory, we can reconstruct the coefficients B_{lm} exactly by integrating over the unit sphere. In fact, for a fixed $r > r_0$, we can write (8) as

$$\hat{p}^r(\theta, \phi) = \sum_{l=0}^{L_0} \sum_{m=-l}^l \hat{p}_{lm}^r \cdot Y_l^m(\theta, \phi), \quad (15)$$

where

$$\hat{p}^r(\theta, \phi) = \hat{p}(r, \theta, \phi), \quad \hat{p}_{lm}^r = B_{lm} \cdot h_l^{(2)}(kr). \quad (16)$$

Consequently,

$$\hat{p}_{lm}^r = \int_0^\pi \int_0^{2\pi} \hat{p}^r(\theta, \phi) Y_l^m(\theta, \phi)^* \sin(\theta) d\phi d\theta. \quad (17)$$

One of the most common ways to arrive at a numerical approximation of this integral is by a quadrature, i.e. we approximate it by a weighted sum over a finite collection of points

$$\{(\theta_1, \phi_1), \dots, (\theta_{N_I}, \phi_{N_I})\} \subset [0, \pi] \times [0, 2\pi] \quad (18)$$

on the unit sphere:

$$\int_0^\pi \int_0^{2\pi} f(\theta, \phi) \sin(\theta) d\phi d\theta \approx \sum_{i=1}^{N_I} w_i \cdot f(\theta_i, \phi_i), \quad w_i \in \mathbb{C}. \quad (19)$$

The theory of quadratures for one-dimensional integrals has a long history and some results can be extended to the two-dimensional case, a noteworthy difference however

is that the distribution of points on the unit sphere alone is a non-trivial problem on its own (see [5]).

We now define the finite-dimensional vector space of spherical harmonics up to degree L as

$$\Pi^L = \text{span} \{Y_l^m : 0 \leq l \leq L, -l \leq m \leq l\}. \quad (20)$$

Inspecting (15), we therefore have $\hat{p}^r \in \Pi^{L_0}$ for each $r > r_0$. Since

$$Y_{l_1}^{m_1} \cdot Y_{l_2}^{m_2} \in \Pi^{l_1+l_2}, \quad (21)$$

we later require a quadrature rule for (17) to be exact at least on Π^{2L_0} .

The most basic scheme that ensures exact integration of all spherical harmonics up to a given degree is a Gaussian product, a repeated application of two one-dimensional quadratures,

$$\sum_{i=1}^{N_I} w_i \sum_{j=1}^{N_J} v_j \cdot f(\theta_i, \phi_j) = \sum_{i=1}^{N_I} \sum_{j=1}^{N_J} \tilde{w}_{ij} \cdot f(\theta_i, \phi_j). \quad (22)$$

It uses an equally spaced scheme (such as the trapezoidal method) in ϕ and Gauss-Legendre scheme for θ . In order to be exact on Π^L with L odd, we would need $(L+1)/2$ nodes for the θ -integral and $(L+1)$ points for the ϕ -integration, yielding a total of $(L+1)^2/2$ points on the sphere (cf. [5]). A common critique of Gaussian products is the inequality of weights and that the distribution of nodes is clustered around the poles (see Figure 1).

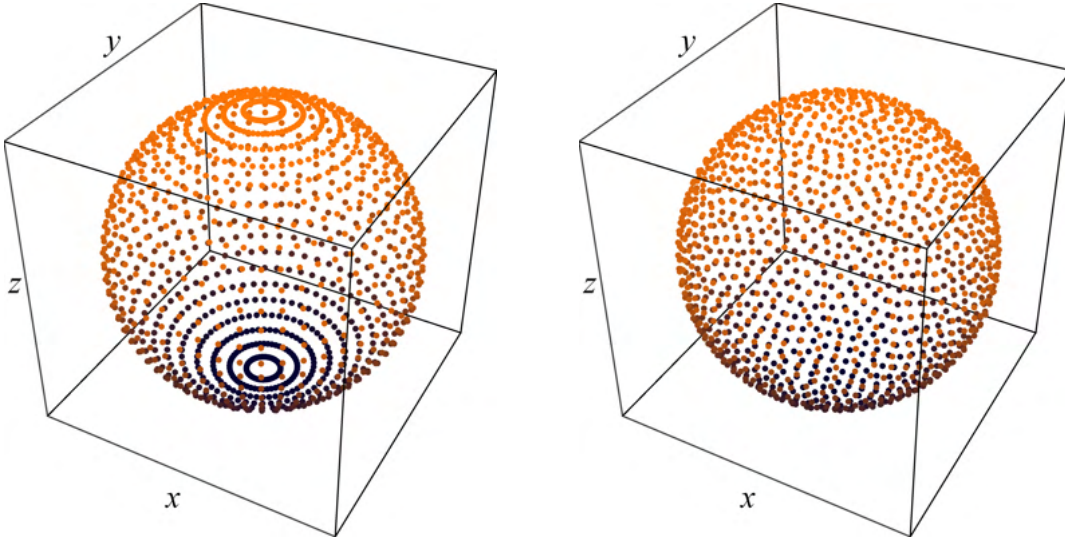


Figure 1: Gaussian product grid of degree $L = 51$ with 1352 nodes (left) and spherical L -design with $L = 51$ and 1328 nodes (right)

If we impose the requirement that a quadrature has equal weights and is exact for all spherical harmonics up to a given degree, we arrive at spherical designs, which were initially defined in [6] as a problem in algebraic combinatorics. A set of points

$$\{(\theta_1, \phi_1), \dots, (\theta_{N_I}, \phi_{N_I})\} \subset [0, \pi] \times [0, 2\pi] \quad (23)$$

is called a spherical L -design if for each $f \in \Pi^L$

$$\int_0^\pi \int_0^{2\pi} f(\theta, \phi) \sin(\theta) d\phi d\theta = \frac{4\pi}{N_I} \sum_{i=1}^{N_I} f(\theta_i, \phi_i). \quad (24)$$

Obviously one wants to construct spherical designs with a minimal amount of nodes, and this is a subject of active research (see [7–9]). For the actual computations of this paper we refer to [10] with accompanying website [11] containing the datasets of symmetric (i.e. antipodal) spherical L -designs of odd degrees up to $L = 325$. Figure 1 shows an example of degree $L = 51$.

1.1.3. Reconstruction method SIFAH

For reconstructing the coefficients B_{lm} we now propose the following. Choose a spherical L -design

$$\{(\theta_1, \phi_1), \dots, (\theta_{N_I}, \phi_{N_I})\} \quad (25)$$

and take a measurement of \hat{p} at the positions

$$(r, \theta_1, \phi_1), \dots, (r, \theta_{N_I}, \phi_{N_I}), \quad (26)$$

all of which are located on a sphere with radius $r > r_0$ in the source-free region. Then, approximate the coefficients via

$$B_{lm} \cdot h_l^{(2)}(kr) \approx \frac{4\pi}{N_I} \sum_{i=1}^{N_I} \hat{p}(r, \theta_i, \phi_i) Y_l^m(\theta_i, \phi_i)^*. \quad (27)$$

This approximation is exact (i.e. (27) is an equation) for degrees

$$l \leq L - L_0. \quad (28)$$

Consequently, \hat{p} can be reconstructed completely by taking $L \geq 2L_0$. Conversely, if only an upper bound for L_0 is known, $L_0 \leq L_{max}$, the above method ensures the exact reconstruction of the first $L - L_{max} + 1$ degrees. For the remainder of this section, we suppose that the degree L of the underlying spherical design is chosen sufficiently large such that (27) is exact.

In most real-life applications, it is not possible to measure \hat{p} in all directions (25) around the sphere. We therefore modify the above method to render partial measurements possible. Let $\hat{p}_1^r, \dots, \hat{p}_M^r$ be a measurement of \hat{p} at the so-called active positions

$$(r, \theta_1, \phi_1), \dots, (r, \theta_M, \phi_M), \quad (29)$$

the corresponding passive positions without any information on \hat{p} being

$$(r, \theta_{M+1}, \phi_{M+1}), \dots, (r, \theta_{N_I}, \phi_{N_I}). \quad (30)$$

Using this decomposition, we analyze the right-hand side of (27):

$$\begin{aligned} \frac{4\pi}{N_I} \sum_{i=1}^{N_I} \hat{p}(r, \theta_i, \phi_i) Y_l^m(\theta_i, \phi_i)^* &= \frac{4\pi}{N_I} \sum_{i=1}^M \hat{p}(r, \theta_i, \phi_i) Y_l^m(\theta_i, \phi_i)^* \\ &\quad + \frac{4\pi}{N_I} \sum_{i=M+1}^{N_I} \hat{p}(r, \theta_i, \phi_i) Y_l^m(\theta_i, \phi_i)^* \end{aligned} \quad (31)$$

$$\begin{aligned} &= \frac{4\pi}{N_I} \sum_{i=1}^M \hat{p}_i^r Y_l^m(\theta_i, \phi_i)^* \\ &\quad + \frac{4\pi}{N_I} \sum_{i=M+1}^{N_I} \sum_{l=0}^{L_0} \sum_{\bar{m}=-l}^l \hat{p}_{i\bar{m}}^r \cdot Y_{i\bar{m}}^{\bar{m}}(\theta_i, \phi_i) Y_l^m(\theta_i, \phi_i)^*. \end{aligned} \quad (32)$$

We therefore obtain

$$\hat{p}_{lm}^r = \frac{4\pi}{N_I} \sum_{i=1}^M \hat{p}_i^r Y_l^m(\theta_i, \phi_i)^* + \frac{4\pi}{N_I} \sum_{i=M+1}^{N_I} \sum_{\bar{l}=0}^{L_0} \sum_{\bar{m}=-\bar{l}}^{\bar{l}} \hat{p}_{i\bar{m}}^r \cdot Y_{\bar{l}}^{\bar{m}}(\theta_i, \phi_i) Y_l^m(\theta_i, \phi_i)^* \quad (33)$$

for each $l \in \{0, \dots, L_0\}$, $m \in \{-l, \dots, l\}$. By introducing

$$x^r = (\hat{p}_{00}^r, \hat{p}_{1-1}^r, \hat{p}_{10}^r, \hat{p}_{11}^r, \dots, \hat{p}_{L_0 L_0}^r) \in \mathbb{C}^{(L_0+1)^2}, \quad (34)$$

$$b^r = (b_{00}^r, b_{1-1}^r, b_{10}^r, b_{11}^r, \dots, b_{L_0 L_0}^r) \in \mathbb{C}^{(L_0+1)^2}, \quad b_{lm}^r = \frac{4\pi}{N_I} \sum_{i=1}^M \hat{p}_i^r Y_l^m(\theta_i, \phi_i)^*, \quad (35)$$

$$A(x^r) = (a_{00}(x^r), a_{1-1}(x^r), a_{10}(x^r), a_{11}(x^r), \dots, a_{L_0 L_0}(x^r)) \in \mathbb{C}^{(L_0+1)^2}, \quad (36)$$

$$a_{lm}(x^r) = \frac{4\pi}{N_I} \sum_{i=M+1}^{N_I} \sum_{\bar{l}=0}^{L_0} \sum_{\bar{m}=-\bar{l}}^{\bar{l}} \hat{p}_{i\bar{m}}^r \cdot Y_{\bar{l}}^{\bar{m}}(\theta_i, \phi_i) Y_l^m(\theta_i, \phi_i)^*, \quad (37)$$

we are able to combine the $(L_0 + 1)^2$ equations of (33) into

$$x^r = b^r + A(x^r) = \mathcal{A}^r(x^r). \quad (38)$$

Consequently, the vector $x^r \in \mathbb{C}^{(L_0+1)^2}$ of coefficients we are trying to reconstruct is a fixed-point of the affine map $\mathcal{A}^r : \mathbb{C}^{(L_0+1)^2} \rightarrow \mathbb{C}^{(L_0+1)^2}$ (A is a linear map). Any reconstruction method based on a fixed-point iteration with \mathcal{A}^r will be called a *SIFAH* method (*Spherical Integration Farfield Acoustical Holography*). Using this notation, equation (27) corresponds to the degenerate case of (38), that is $x^r = b^r$ or, equivalently,

$$\mathcal{A}^r(x^r) = b^r = \text{const.} \quad (39)$$

In this case, a SIFAH iteration would converge in just one step to a fixed point regardless of how the starting point $x_0^r \in \mathbb{C}^{(L_0+1)^2}$ is chosen.

Finally, this approach can easily be generalized to allow for active positions with varying radii (e.g. planar measurements) in the source-free region. Due to the limited scope of this article, a derivation of the corresponding formulas will be part of a future publication.

2. SIMULATION OF SPHERICAL CAP PISTONS

A vibrating spherical cap piston with aperture angle $\alpha \in (0, 2\pi]$ centered on the north pole of an otherwise rigid sphere with radius r_0 can be described by its surface velocity

$$v^\alpha : [0, \pi] \times [0, 2\pi] \rightarrow \mathbb{R}, \quad v^\alpha(\theta, \phi) = V \cdot a^\alpha(\theta, \phi), \quad V \in \mathbb{R}, \quad (40)$$

the corresponding aperture function $a^\alpha : [0, \pi] \times [0, 2\pi] \rightarrow \mathbb{R}$ is given by

$$a^\alpha(\theta, \phi) = 1 - H\left(\theta - \frac{\alpha}{2}\right), \quad H(x) = \begin{cases} 0 & x < 0 \\ 1 & x \geq 0 \end{cases}. \quad (41)$$

The spherical wave spectrum of v^α ,

$$v^\alpha(\theta, \phi) = \sum_{l=0}^{\infty} \sum_{m=-l}^l v_{lm}^\alpha \cdot Y_l^m(\theta, \phi), \quad (42)$$

can be computed via

$$v_{lm}^\alpha = V \delta_{m0} \sqrt{(2l+1)\pi} \int_{\cos(\frac{\alpha}{2})}^1 P_l^0(x) dx. \quad (43)$$

Rotating the spherical cap to be centered in the direction $(\tilde{\theta}, \tilde{\phi})$ results in

$$\tilde{v}_{lm}^\alpha = \sqrt{\frac{4\pi}{2l+1}} Y_l^m(\tilde{\theta}, \tilde{\phi})^* \cdot v_{lm}^\alpha, \quad (44)$$

respectively. Finally, the radiated pressure in the source-free region is completely determined by the surface velocity spectrum (see for example [12]):

$$\hat{p}_{v^\alpha}(r, \theta, \phi) = -i\rho_0 c \sum_{l=0}^{\infty} \sum_{m=-l}^l \frac{h_l^{(2)}(kr)}{h_l^{(2)'}(kr_0)} v_{lm}^\alpha \cdot Y_l^m(\theta, \phi). \quad (45)$$

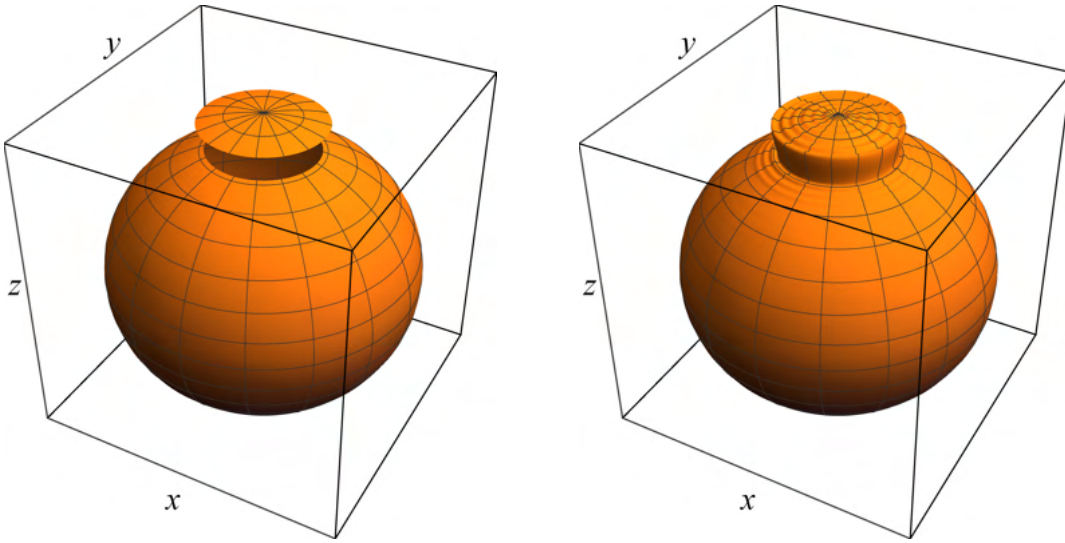


Figure 2: Radial plot of v^α for $\alpha = 40^\circ$ (left) and its spherical wave expansion up to degree $L = 120$ (right)

2.2.1. Smooth spherical pistons

As hinted at in Figure 2, most of the higher degrees in the expansion (42) of v^α are present to form the discontinuity at the boundary of the spherical cap. In order to avoid this discontinuity, we also introduce a smooth one-parameter family of spherical pistons with surface velocity

$$w^\alpha : [0, \pi] \times [0, 2\pi] \rightarrow \mathbb{R}, \quad w^\alpha(\theta, \phi) = V \cdot \exp\left(-\frac{(1 - \cos(\theta))^2}{\left(1 - \cos\left(\frac{\alpha}{2}\right)\right)^2}\right). \quad (46)$$

Again, we will call α the aperture angle of this piston, but now, when varying θ from 0 to $\alpha/2$, the particle velocity smoothly changes from V to V/e . As before, the spherical wave spectrum of w^α can be determined by one-dimensional integration (see Figure 3 and Figure 4):

$$w_{lm}^\alpha = V\delta_{m0}\sqrt{(2l+1)\pi}\int_{-1}^1 P_l^0(x)\exp\left(-\frac{(1-x)^2}{(1-\cos(\frac{\alpha}{2}))^2}\right)dx. \quad (47)$$

Moreover, transformation rule (44) also holds for the coefficients w_{lm}^α when rotating the smooth spherical piston to be centered in the direction $(\tilde{\theta}, \tilde{\phi})$, and the radiated sound pressure \hat{p}_{w^α} corresponding to w^α can be computed in complete analogy to (45).

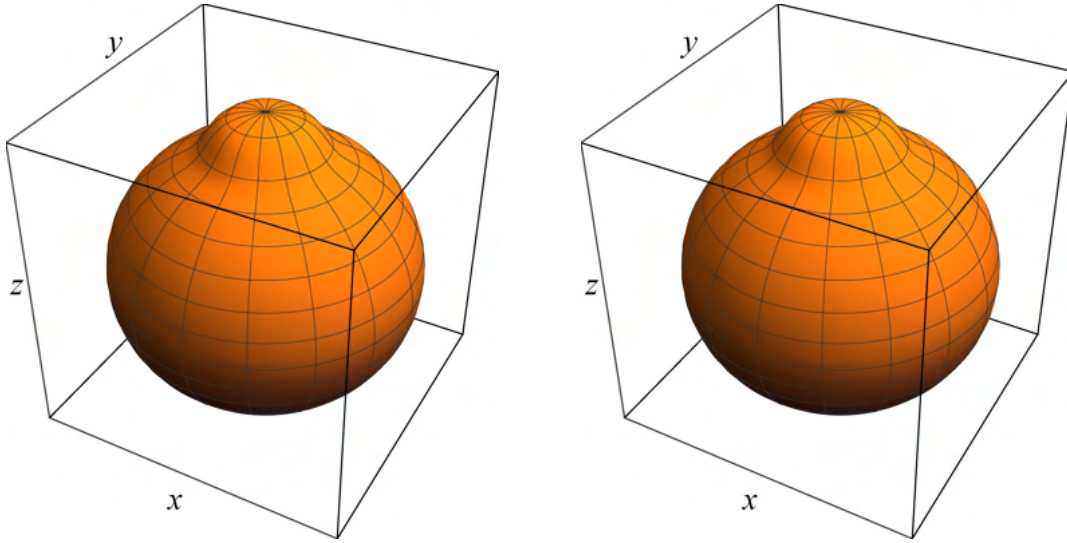


Figure 3: Radial plot of w^α for $\alpha = 40^\circ$ (left) and its spherical wave expansion up to degree $L = 120$ (right)

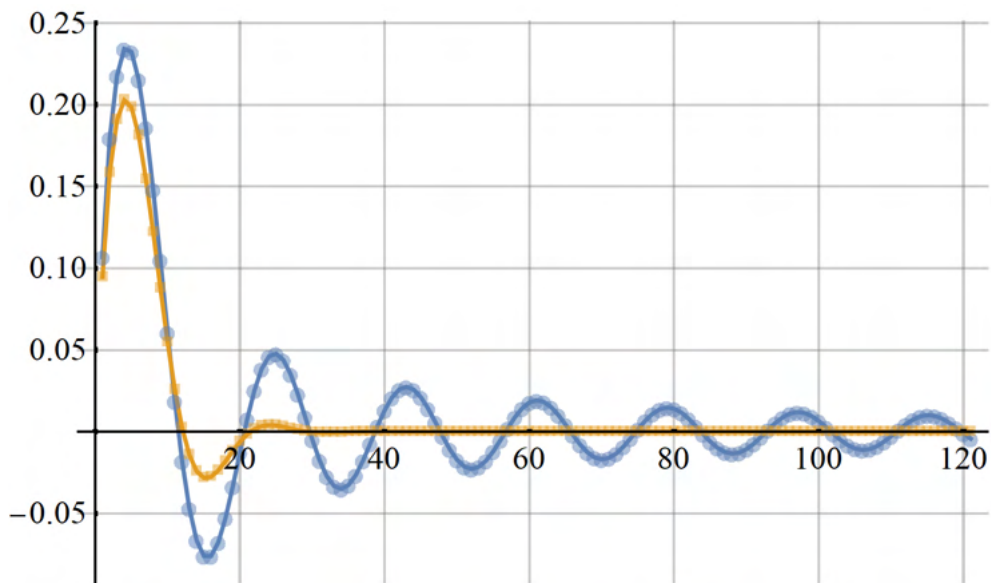


Figure 4: Coefficients v_{l0}^α (blue circles) and w_{l0}^α (yellow boxes) for $\alpha = 40^\circ$ in units of V

3. RESULTS

To exemplify the capability of SIFAH, we now reconstruct the simulated sound pressure field generated by one or more (smooth) spherical pistons vibrating at $r_0 = 2.5$ m. The simulation degree is 120 (cf. Figures 2, 3 and 4). In order to determine/reconstruct degrees up to $L_0 = 25$, we pick the symmetric spherical L -design with $L = 51$ listed in [11], scale it to the radius $r = 4$ m and decompose it into 222 active and 1106 passive positions (see Figures 1 and 5), the former are defined by

$$(\theta, \phi) \in [60^\circ, 120^\circ] \times [30^\circ, 150^\circ]. \quad (48)$$

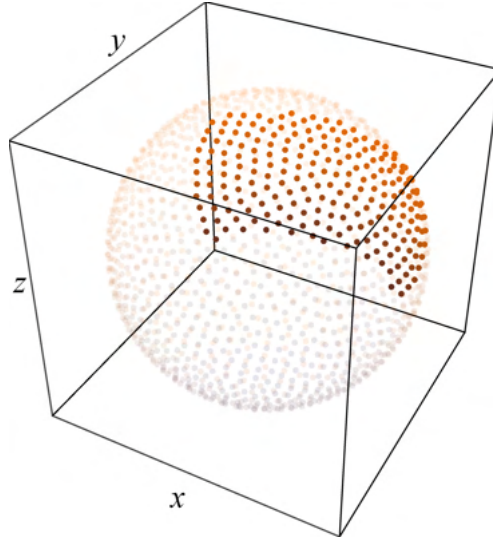


Figure 5: Symmetric spherical L -design with $L = 51$ decomposed into 222 active positions (solid) and 1106 passive positions (transparent)

Using the simulated pressures at the active positions, we then apply the SIFAH method. The starting point of the SIFAH fixed-point iteration is

$$x_0^r = 0 \in \mathbb{C}^{(L_0+1)^2}, \quad (49)$$

its maximal number of steps is 500. Finally, the resulting vector of coefficients is used to reconstruct the sound pressure in the plane defined by

$$(x, y, z) \in [-8 \text{ m}, 8 \text{ m}] \times [8 \text{ m}] \times [-1 \text{ m}, 1 \text{ m}]. \quad (50)$$

In the first example, we simulate a spherical cap piston with aperture angle $\alpha = 90^\circ$ centered in the direction $(0, 1, 0)$ (see section 2). For each of the considered frequencies $f = 250$ Hz, 500 Hz, 1000 Hz, both the simulated and the reconstructed pressures clearly exhibit the limited number of simulation degrees (see Figures 6, 7 and 8).

Using the same aperture angle, direction and frequencies, we then simulate a smooth spherical piston as our second example (see subsection 2.1). Now, simulation and reconstruction are in excellent agreement with each other (see Figures 9, 10 and 11). Moreover, under the given limit of simulation degrees, this one-parameter family of pistons seems to be well-suited for modeling directional sources.

Therefore, the third and final example consists of four smooth spherical pistons (each of the same maximal surface velocity V), the directions and aperture angles of which are

$$(\theta_1, \phi_1, \alpha_1) = (80^\circ, 110^\circ, 20^\circ), \quad (\theta_2, \phi_2, \alpha_2) = (100^\circ, 30^\circ, 100^\circ), \quad (51)$$

$$(\theta_3, \phi_3, \alpha_3) = (95^\circ, 120^\circ, 40^\circ), \quad (\theta_4, \phi_4, \alpha_4) = (100^\circ, 90^\circ, 15^\circ). \quad (52)$$

The frequencies under consideration are $f = 250$ Hz, 1000 Hz, 4000 Hz. As the linear nature of the approach suggests, the SIFAH method successfully reconstructs the sound pressure field for this superposition of directional sources (see Figures 12, 13 and 14).

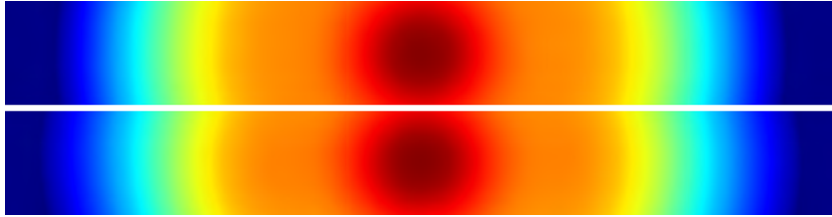


Figure 6: Pressure magnitude (12 dB), single spherical cap piston, $f = 250$ Hz, simulation of degree 120 (top) and SIFAH reconstruction of degree 25 (bottom)

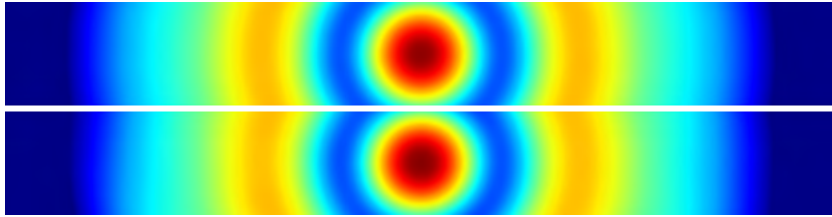


Figure 7: Pressure magnitude (12 dB), single spherical cap piston, $f = 500$ Hz, simulation of degree 120 (top) and SIFAH reconstruction of degree 25 (bottom)

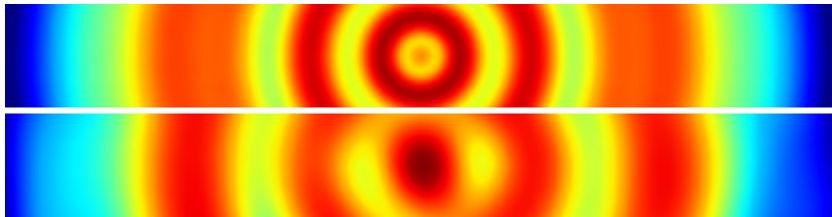


Figure 8: Pressure magnitude (12 dB), single spherical cap piston, $f = 1000$ Hz, simulation of degree 120 (top) and SIFAH reconstruction of degree 25 (bottom)

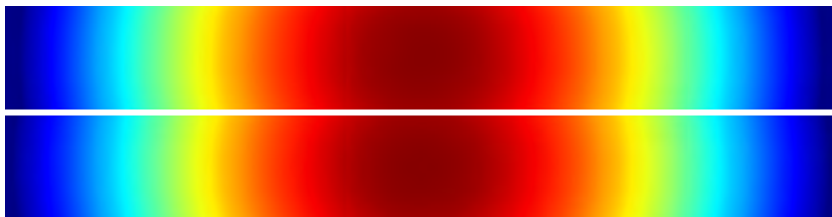


Figure 9: Pressure magnitude (12 dB), single smooth spherical piston, $f = 250$ Hz, simulation of degree 120 (top) and SIFAH reconstruction of degree 25 (bottom)

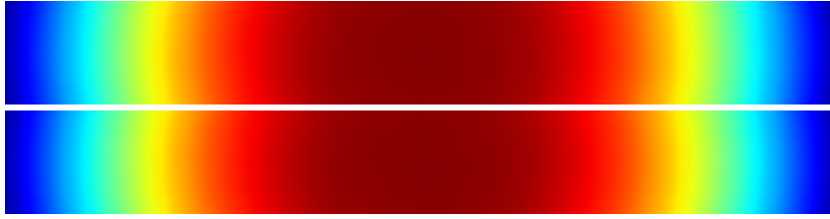


Figure 10: Pressure magnitude (12 dB), single smooth spherical piston, $f = 500$ Hz, simulation of degree 120 (top) and SIFAH reconstruction of degree 25 (bottom)



Figure 11: Pressure magnitude (12 dB), single smooth spherical piston, $f = 1000$ Hz, simulation of degree 120 (top) and SIFAH reconstruction of degree 25 (bottom)

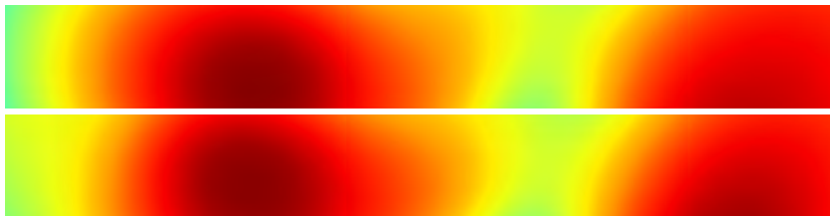


Figure 12: Pressure magnitude (12 dB), multiple smooth spherical pistons, $f = 250$ Hz, simulation of degree 120 (top) and SIFAH reconstruction of degree 25 (bottom)

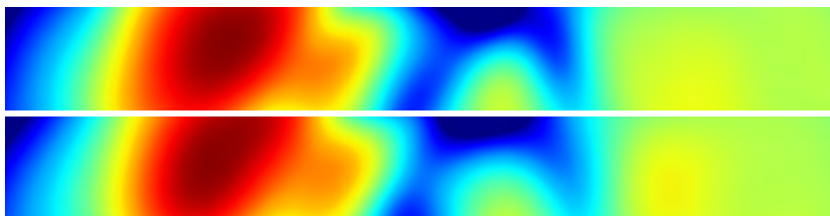


Figure 13: Pressure magnitude (12 dB), multiple smooth spherical pistons, $f = 1000$ Hz, simulation of degree 120 (top) and SIFAH reconstruction of degree 25 (bottom)

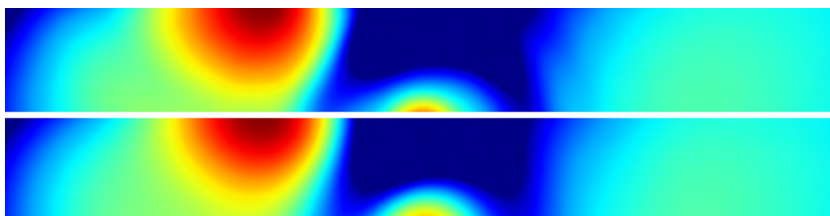


Figure 14: Pressure magnitude (12 dB), multiple smooth spherical pistons, $f = 4000$ Hz, simulation of degree 120 (top) and SIFAH reconstruction of degree 25 (bottom)

4. ACKNOWLEDGEMENTS

This research work has been funded by German Federal Ministry for Economic Affairs and Energy (Bundesministerium für Wirtschaft und Energie BMWi) under project

MeKariS registration number MF 160166.

REFERENCES

- [1] A. Sommerfeld, *Partial differential equations in physics*, Pure and Applied Mathematics, vol. 1, Academic Press, New York, 1949. ↑2
- [2] S.F. Wu, *The Helmholtz equation least squares method*, Modern Acoustics and Signal Processing, Springer, New York, 2015. ↑2, 3
- [3] E.G. Williams, *Regularization methods for near-field acoustic holography*, Journal of the Acoustical Society of America **110** (2001), no. 4, 1976–1988. ↑3
- [4] G.H. Golub, M. Heath, and G. Wahba, *Generalized cross-validation as a method for choosing a good ridge parameter*, Technometrics **21** (1979), no. 2, 215–223. ↑3
- [5] C.H.L. Beentjes, *Quadrature on a spherical surface*, Mathematical Institute, University of Oxford, Oxford, UK, 2015. ↑4
- [6] P. Delsarte, J.M. Goethals, and J.J. Seidel, *Spherical codes and designs*, Geometriae Dedicata **58** (1977), 363–388. ↑4
- [7] R.H. Hardin and N.J.A. Sloane, *Mclarens improved snub cube and other new spherical designs in three dimensions*, Discrete & Computational Geometry **15** (1996), 429–441. ↑5
- [8] E. Bannai, *A survey on spherical designs and algebraic combinatorics on spheres*, European Journal of Combinatorics **30** (2009), 1392–1425. ↑5
- [9] J.S. Brauchart and P.J. Grabner, *Distributing many points on spheres: Minimal energy and designs*, Journal of Complexity **31** (2015), 293–326. ↑5
- [10] R.S. Womersley, *Efficient spherical designs with good geometric properties*, Contemporary Computational Mathematics - A Celebration of the 80th Birthday of Ian Sloan, 2018, pp. 1243–1285. ↑5
- [11] ———, *Symmetric spherical designs on the sphere \mathbb{S}^2 with good geometric properties*, <http://web.maths.unsw.edu.au/~rsw/Sphere/EffSphDes/>. Accessed: 2019-02-28. ↑5, 9
- [12] E.G. Williams, *Fourier acoustics: sound radiation and nearfield acoustical holography*, Academic Press, 1999. ↑7